Journal of Materials Chemistry C

Check for updates

Realization of deep-blue TADF in sterically controlled naphthyridines for vacuum- and solution-processed OLEDs†

Gediminas Kreiza, [a] Dovydas Banevičius, [a] Justina Jovaišaitė, [a]
Saulius Juršėnas, [a] Tomas Javorskis, [b] Vytenis Vaitkevičius, [b] Edvinas Orentas [b] and
Karolis Kazlauskas ⋆[a]

Narrow-band deep-blue (emission peak < 460 nm) TADF emitters are in demand for commercial OLED display applications, yet the development of efficient emitters with low efficiency roll-off is very challenging. To address this issue, herein, we studied carbazole–naphthyridine (donor–acceptor)-based blue-emitting TADF compounds, which were designed by using both the H-bonding and sterically controlled charge-transfer (CT) interactions between D and A units. Methyl substitution employed at the first position of *t*-butyl-carbazole donors was found to affect CT strength and consequently the TADF properties of the studied compounds, enabling a significant reduction of delayed fluorescence lifetime (down to 3.1 μs) and enhancement of reverse intersystem crossing rate (up to 10^6 s^{-1}). The naphthyridines were demonstrated to hold great potential as deep-blue TADF emitters suitable for both vacuum- and solution-processed TADF OLEDs. The optimized devices with 7 wt% naphthyridine emitter in a weakly polar mCP host delivered external quantum efficiencies (EQEs) of up to ∼17.6% and ∼13.5% for vacuum- and solution-processed OLEDs, respectively. Unsubstituted naphthyridine exhibited deep-blue (λ_{max} < 460 nm) and narrow-band (FWHM = 66 nm) electroluminescence, whereas the more twisted methyl-substituted compound expressed broader band (FWHM > 80 nm) sky-blue (λ_{max} ≈ 480 nm) emission. The demonstrated emitters are among the best-performing conventional D–A-type blue/deep-blue TADF emitters in terms of EQE and efficiency roll-off properties of their devices.

1. Introduction

The basic design principles of high performance thermally activated delayed fluorescence (TADF) compounds routinely rely on the combination of spatially twisted donor (D) and acceptor (A) moieties.[1] This enables large separation of the highest occupied (HOMO) and lowest unoccupied (LUMO) molecular orbitals subsequently resulting in a small energy gap between the lowest excited singlet (S_1) and triplet (T_1) states. The twisted D–A compounds express charge-transfer (CT) character and are highly attractive for organic light emitting diode (OLED) applications due to the potentially fast and efficient reverse intersystem crossing (rISC).[2] It allows the utilization of both singlet and triplet excitons formed in the emitting layer of a device after

electron and hole injection.[3] Although TADF-based OLEDs are frequently reported to reach 100% internal quantum efficiency,[4] their application in commercial displays is limited by their broadened (FWHM ∼ 90 nm) and red-shifted fluorescence (FL) spectra due to the strong intramolecular CT and conformational disorder caused by variation in the twisting angle between D and A moieties.[5] Therefore, the development of efficient narrow-band (FWHM < 60 nm) TADF emitters is considered to be a challenging task, especially for the blue/deep-blue OLEDs.[6,7]

The reported approaches to achieve narrow blue TADF rely on rigid sterically hindered[8] or donor-interlocked molecular structures,[9] HOMO–LUMO separation by the multiple resonance effect[10] and weak CT compounds.[11] An additional involvement of H-bonding interactions between nitrogen heteroatoms in A and neighbouring C–H bonds in D units was also found to facilitate delivering narrow blue TADF emission.[12] It seems that the combination of both H-bonding and CT interactions in a controlled manner could be an attractive strategy to achieve high-performance blue OLEDs, and more importantly, to gain understanding of the TADF mechanism of D–A systems containing nitrogen heteroatoms in their building blocks.

[a] *Institute of Photonics and Nanotechnology, Vilnius University, Saulėtekio av. 3, LT-10257 Vilnius, Lithuania. E-mail: karolis.kazlauskas@ff.vu.lt*

[b] *Department of Organic Chemistry, Vilnius University, Faculty of Chemistry and Geosciences, Naugarduko 24, Vilnius LT-03225, Lithuania*

† Electronic supplementary information (ESI) available. CCDC 1991494 and 1992697. For ESI and crystallographic data in CIF or other electronic format see DOI: 10.1039/d0tc01637c
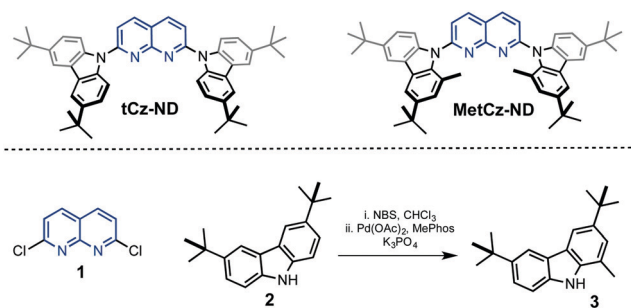
Fig. 1 Chemical structures of the synthesized 1,8-naphthyridine (ND) derivatives and precursors 1–3.

Recently, a nitrogen heteroatom-containing naphthyridine acceptor was successfully utilized in the construction of TADF emitters.[13–16] The combination of naphthyridine with a variety of donors, e.g. those based on acridane, carbazole, phenoxazine and phenothiazine regularly employed for designing efficient TADF compounds, produced yellow/green/blue emitters with peak wavelength (λ_{max}) above 460 nm. Meanwhile, implementing them in efficient OLEDs produced surprisingly low external quantum efficiency (EQE) roll-offs.[15,16] Note, however, that for commercial applications like OLED displays, narrow-band deep-blue emitters with $\lambda_{max} < 460$ nm are required.[17] To reveal the potential of naphthyridine acceptors for the formation of deep-blue TADF emitters, we have designed a couple of 1,8-naphthyridine (ND)-based compounds with tert-butyl-carbazole (tCz) serving as the donor (Fig. 1). Although one of the compounds, **tCz-ND,** was recently reported,[16] its most intriguing photophysical properties and its possibilities to be employed in deep-blue OLEDs remained overlooked. Herein, **tCz-ND** was also used for comparative analysis with the second compound **MetCz-ND** containing additional methyl (Me) moieties at the first position of the tCz donors. Me substitution was employed to alter steric hindrance and, consequently, twisting of the D and A units. The modification permitted assessing the impact of intramolecular D–A interaction and CT strength on TADF properties of the studied compounds and on their performance in both solution- and vacuum-processed OLEDs.

2. Experimental section

2.1. Sample preparation and instrumentation

Absorption spectra of dilute toluene solutions (10^{-5} M) of the investigated naphthyridine derivatives were recorded using a Lambda 950 UV-vis-NIR spectrophotometer (PerkinElmer). 1,3-Bis(N-carbazolyl)benzene (mCP) films doped with 7 wt% contents of the compounds were prepared by spin-coating chloroform solutions (20 mg mL^{-1}) of mCP and compound mixtures on quartz substrates at 2000 rpm and annealing at 50 °C for 20 minutes to remove residual solvent. Steady state PL spectra were recorded using a PMA-12 back-thinned CCD spectrometer (Hamamatsu) by exciting samples with a xenon lamp coupled to a monochromator. Toluene solutions were degassed by the freeze–pump–thaw method. Fluorescence quantum yield (Φ_{FL})

was estimated in oxygen-free media by using the integrating sphere (Sphere Optics) and comparative methods for solutions, where quinine sulfate in 0.1 M H_2SO_4 served as the reference.[18] All samples were excited at 340 nm. FL transients were measured using an NT 242 nanosecond YAG:Nd^{3+} laser equipped with an optical parametric oscillator (Ekspla, excitation wavelength 340 nm, pulse duration 5 ns, and repetition rate 1 kHz) and an iStar DH340T time-gated intensified CCD camera (Andor) mounted on an SR-303i spectrograph (Shamrock). Measurements at low temperatures were performed in a 204N closed-cycle helium cryostat (Cryo Industries). Ionization potential (I_p) of the wet-casted films was estimated by photoelectron emission spectrometry in air.[19] The films for the measurements were prepared by dissolving materials in THF and by casting the solutions on polyester film coated with an Al conductive layer and ∼0.5 μm-thick methylmethacrylate and methacrylic acid copolymer adhesive layers. Prior to experiments, the investigated compounds were purified using a DSU-20 vacuum sublimation system (CreaPhys).

2.2. OLED fabrication and characterization

OLEDs were fabricated on pre-patterned ITO/glass substrates (purchased from Kintec company). ITO layer thickness was 100 nm with a sheet resistance of 15–20 Ω □$^{-1}$. Prior to device fabrication, the substrates were cleaned by ultrasonication in a detergent (Hellmanex II) at 50 °C for 10 minutes; then, substrates were rinsed with running distilled water and blow-gunned ensuring no residual detergent is left. Afterwards, the substrates were sonicated consecutively in distilled water, acetone and isopropyl alcohol for 15 minutes (in each solvent). Immediately after the substrates were removed from the iso-propanol bath, they were immersed in boiling hot distilled water and then dried. The substrates were then treated with O_2 plasma and transferred into a nitrogen-filled glovebox with an integrated vacuum evaporation chamber. The vacuum-processed devices were fabricated in a vacuum chamber (at a base pressure of $<10^{-6}$ Torr) by depositing multiple organic layers at a rate of 0.5–1.2 Å s^{-1}. The doped emissive layer was obtained by co-evaporating materials from two different evaporation sources at different evaporation rates for the desired doping concentration.

The solution-processed devices were fabricated by the following procedure. O_2 plasma-treated ITO/glass substrates were coated with a PEDOT:PSS (poly(3,4-ethylenedioxythiophene)-poly(styrene-sulfonate)) layer by spin-coating from a water solution at 5000 rpm. Before the coating, PEDOT:PSS (Al 4083, purchased from Ossila) was ultrasonicated and filtered through a 0.45 μm PES filter. The spin-coating resulted in a 40 nm-thick film, which was annealed at 200 °C for 10 minutes to remove residual H_2O. Samples were then transferred into a nitrogen glovebox, where PVK (poly(9-vinylcarbazole)) was spin-coated at 2000 rpm from 6 mg mL^{-1} chlorobenzene solution, and annealed afterwards at 160 °C for 15 min resulting in a 15 nm-thick layer. Immediately after that, a 25 nm-thick emissive layer from a 2.5 mg mL^{-1} cyclohexane solution (emitter : host ratio of 7 : 93 by weight) was spin-coated on top at 1500 rpm. The samples were then left to dry for 30 minutes at room temperature before their transfer to an

This journal is © The Royal Society of Chemistry 2020

J. Mater. Chem. C, 2020, 8, 8560–8566 | 8561

integrated vacuum chamber for further deposition of 5 nm-thick DPEPO (bis[2-(diphenylphosphino)phenyl] ether oxide) followed by a 50 nm-thick TmPyPB (1,3,5-tri(m-pyridin-3-ylphenyl)benzene) layer.

Finally, for both the solution- and vacuum-processed devices, the samples were transferred from the organic deposition chamber to a metal deposition chamber without breaking the vacuum, where (lithium fluoride) LiF and Al layers at the rates of 0.2 and 1.8 Å s^{-1}, respectively, were successively deposited. The active area of the final devices was 1 mm^2, 4 mm^2 or 16 mm^2 as defined by the cross-section of the patterned ITO anode and the shadow mask of cathode deposition. Before exposure to air, the devices were transferred from the vacuum chamber to a nitrogen atmosphere for encapsulation. The OLEDs were encapsulated using a UV-curable epoxy resin (DELO KATIOBOND LP655) and a cover glass on top.

A calibrated characterization set-up comprising an integrating sphere (Lab sphere), a photonic multichannel analyzer PMA-11 (Hamamatsu) and a source meter 2601A (Keithley) was employed to evaluate current–voltage–luminance characteristics and the EQE of the fabricated OLEDs.

3. Results and discussion

3.1. Synthesis

1,8-Naphthyridine derivatives *t*Cz-ND and Me*t*Cz-ND were synthesized in one step from a common precursor, 2,7-dichloro-1,8-naphthyridine 1, and carbazole derivatives 2–3 possessing *tert*-butyl groups using Pd catalysed amination or nucleophilic aromatic substitution reactions, respectively (Fig. 1). The detailed information about the synthetic procedures and identification of molecular structures is provided in the ESI.† The methyl group-containing carbazole 3 was synthesized in high yield using a Suzuki coupling reaction between the corresponding 1-bromo-3,7-di-*tert*-butyl-9*H*-carbazole and methylboronic acid. The structures of *t*Cz-ND and Me*t*Cz-ND were unambiguously confirmed by X-ray analysis (see ESI†). The ND compounds were purified by vacuum sublimation prior to experiments and device fabrication. Thermogravimetry analysis (TGA) of *t*Cz-ND and Me*t*Cz-ND revealed high decomposition temperatures of 433 °C and 422 °C, respectively, implying high thermal stability of both compounds and thus suitability for practical applications (see Fig. S2, ESI†).

3.2. DFT calculations

To gain insight into the photophysical properties of the synthesized compounds, their excitation energies, oscillator strengths, D–A dihedral angles and HOMO and LUMO distributions were calculated by using DFT at the B3LYP/6-31G(d) level (see Table S2 in ESI† and Fig. 2).[20] The unmodified *t*Cz-ND demonstrated rather weak CT character due to the small dihedral angle (31°) between *t*Cz donor and ND acceptor. As expected, Me substituents in Me*t*Cz-ND imposed larger steric hindrance (dihedral angle 55°) resulting in considerably increased CT strength and thus reduced excitation energy, oscillator strength and ΔE_{ST}. Furthermore, analysis of molecular structures in optimized ground state geometries revealed proximity between the N atoms
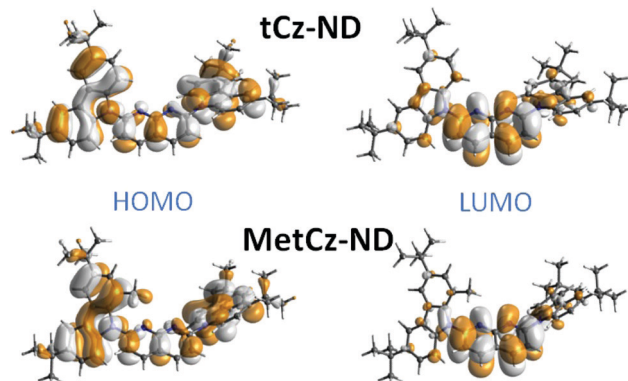

Fig. 2 HOMO and LUMO distributions in 1,8-naphthyridine derivatives calculated by TD-DFT.

of the ND acceptor and the nearest H atoms of neighbouring D groups in both compounds, similarly to previously reported di(pyridinyl)methanone-based TADF emitters.[12] C–H···N distances of 2.39 Å and 2.42 Å for *t*Cz-ND and Me*t*Cz-ND, respectively, were determined, suggesting an involvement of intramolecular H-bonding interactions expected to increase the rigidity of the investigated compounds and thus impact their photophysical properties.

3.3. Photophysical properties

Absorption spectra of the investigated ND derivatives in toluene solutions were found to be in good agreement with the DFT calculation results (see Fig. 3), *i.e.* *t*Cz-ND expressed intense
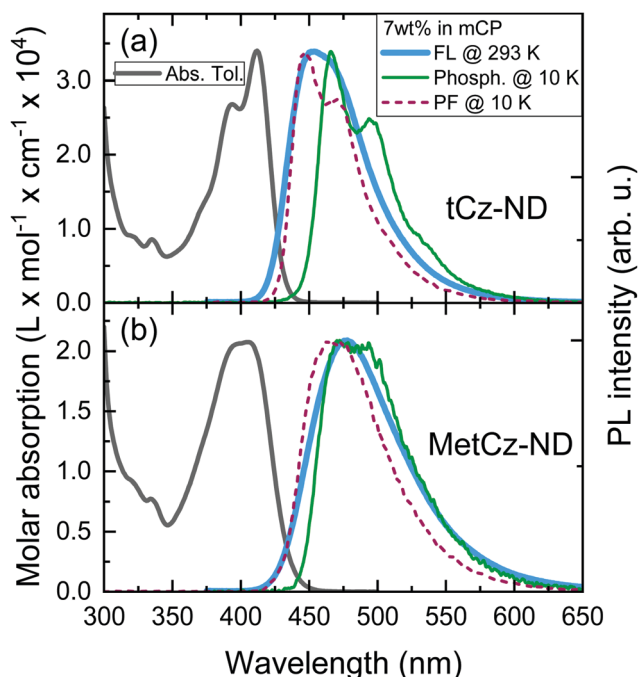

Fig. 3 Absorption (in toluene), fluorescence and phosphorescence spectra (in mCP, and an oxygen-free environment) of *t*Cz-ND (a) and Me*t*Cz-ND (b) at room temperature and 10 K. Prompt FL spectra at 10 K are also shown.

8562 | *J. Mater. Chem. C*, 2020, **8**, 8560–8566

This journal is © The Royal Society of Chemistry 2020

absorption with well-resolved vibronic structure, indicating weak CT character and a less-twisted molecular geometry, whereas **MetCz-ND** exhibited a less structured spectrum with 1.5-fold reduced oscillator strength likely due to enhanced CT and electron-vibronic coupling. Similarly, the FL spectrum of **MetCz-ND** in toluene was structureless and redshifted with respect to that of **tCz-ND**, signifying enhanced CT character (Fig. S3, ESI†). This was additionally verified by estimating the spectral responses of ND compounds with increasing solvent polarity (Fig. S4, ESI†). The change of the polarity from non-polar (cyclohexane) to highly polar (acetonitrile) resulted in a strong red shift and broadening of the FL spectra, which were obviously more pronounced for **MetCz-ND** than for **tCz-ND**. The photophysical properties of ND compounds are summarized in Table S3 (ESI†).

All the studied compounds demonstrated oxygen-sensitive FL in solutions with distinct prompt (PF) and delayed (DF) FL components, signifying the presence of TADF (Fig. 4). Moderately
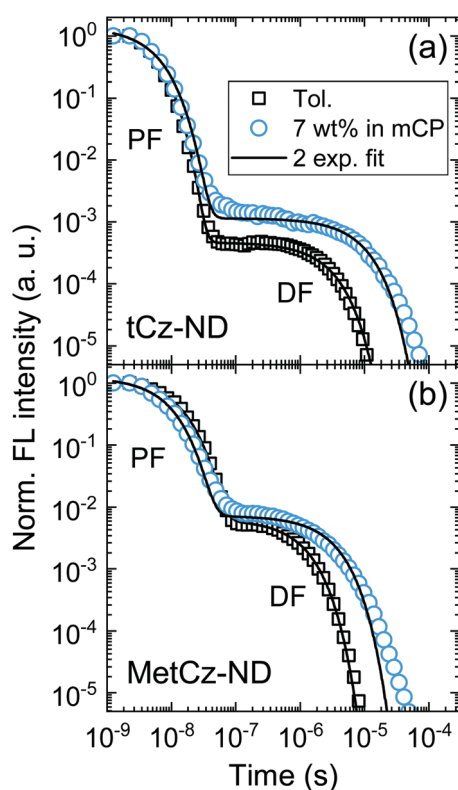
high FL quantum yield (Φ_{FL}) values of 0.53 and 0.64 obtained for **tCz-ND** and **MetCz-ND**, respectively, in solutions were increased up to 0.76 and 0.86, respectively, by dispersing ND derivatives in a rigid mCP host at 7 wt% concentration. This concentration was found to be optimal for the devices delivering maximal EQE. The ND-doped mCP film processing method, *i.e.* vacuum or solution process, was found to have no impact on the Φ_{FL} values. The improved Φ_{FL} values of the compounds in mCP were accompanied by notably enhanced contributions of the DF components (Table 1 and Table S3, ESI†), implying reduced non-radiative decay from the triplet states most likely due to suppressed vibronic coupling to the ground state.[21] The vibronically-modulated prompt FL and phosphorescence spectra of **tCz-ND** in mCP obtained at 10 K again confirmed the origin of the emissive states to be of a more localized (and less CT) nature. Conversely, the analogous spectra of **MetCz-ND** with redshifted structureless emission clearly indicated the CT-like origin of the states (Fig. 3).

DF and PF lifetimes (τ_{DF} and τ_{PF}) in different media were obtained by fitting the transients with double exponential decay profiles (Fig. 4). Slight deviation of the experimental DF points from the fits in the mCP host at the latest times could arise due to the small conformational disorder of the molecular geometry in the solid film.[5] The determined lifetimes along with Φ_{FL} and DF/PF ratios were further used to calculate the rISC rate (k_{rISC}) according to the previously described procedures assuming that non-radiative decay occurs mainly from the triplet states (as discussed above).[21] The revealed k_{rISC} was found to be 3-fold larger for **MetCz-ND** (1.06×10^6 s^{-1} in mCP) as compared to that of the unmodified **tCz-ND** (0.34×10^6 s^{-1} in mCP), which could be a result of the enhanced coupling between S$_1$ and T$_1$ due to the small ΔE_{ST} (0.09 eV) and stronger vibronic coupling because of the more labile molecular structure. On the other hand, less structurally twisted **tCz-ND** showed the highest radiative decay rate ($k_r = 4.4 \times 10^7$), which, accompanied with a deep blue ($\lambda_{max} = 452$ nm) and narrow (FWHM = 66 nm) FL spectrum, makes **tCz-ND** an excellent candidate for pure blue emitting TADF-OLEDs.

3.4. OLED performance

To evaluate the potential of naphthyridine compounds as blue TADF emitters for OLED applications, their electroluminescence (EL) properties were studied. The two ND compounds were compared in the same device architecture, where they were employed as dopants in the ND:mCP emissive layer at the same optimal doping concentration (7 wt%), identical to that used for FL studies (Fig. 3 and 4). Under such conditions, the obtained device characteristics including efficiency roll-off could be directly linked to the molecular properties of the ND compounds.

Fig. 4 FL decay transients of **tCz-ND** (a) and **MetCz-ND** (b) in toluene (squares) and the mCP host at 7 wt% doping concentration (circles) in an oxygen-free environment. Solid lines represent double exponential fits. PF and DF components are indicated.

Table 1 Photophysical properties of the investigated naphthyridine-doped mCP films (7 wt%) prepared by the solution-process

Compd.	λ_{max} (nm)	Φ_{FL}	Φ_{DF}/Φ_{PF}[a]	τ_{PF} (ns)	τ_{DF} (µs)	k_r (10^7 s^{-1})	k_{ISC} (10^7 s^{-1})	k_{rISC} (10^6 s^{-1})	ΔE_{ST}[b] (eV)	HOMO/LUMO[c] (eV)
tCz-ND	452	0.76	0.53/0.23	5.2	8.8	4.4	14.8	0.34	0.18	5.6/2.7
MetCz-ND	478	0.86	0.61/0.25	8.3	3.1	3.0	9.0	1.06	0.09	5.6/2.7

[a] Estimated from the FL transient measurements. [b] ΔE_{ST} estimated from the onsets of FL (@293 K) and phosphorescence (@10 K) spectra. [c] HOMO obtained from ionization potential measured by photoelectron emission spectrometry; LUMO = HOMO − E_g.

This journal is © The Royal Society of Chemistry 2020

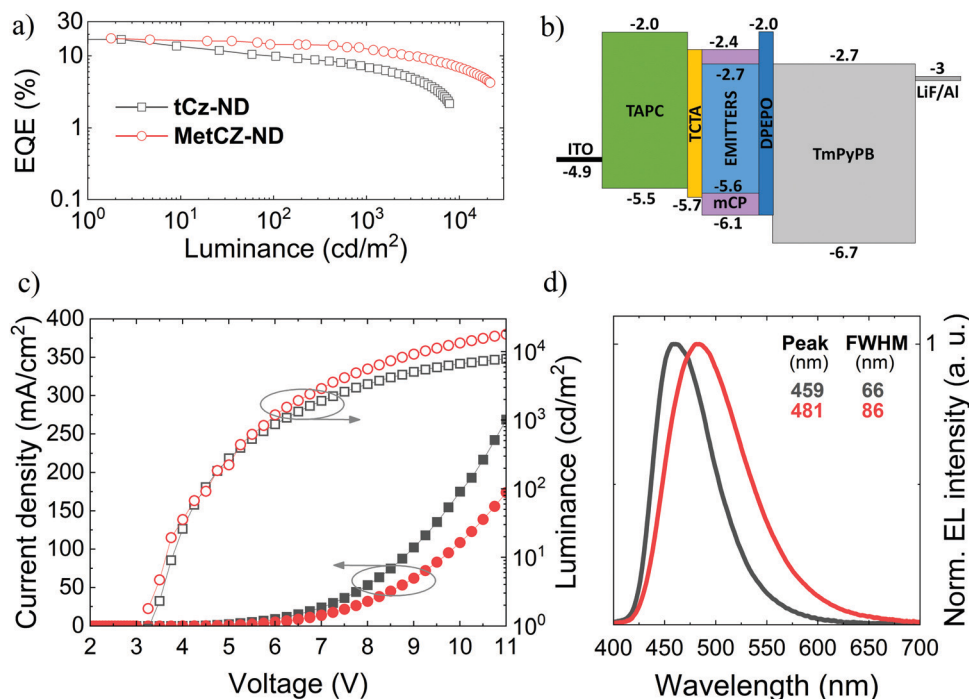*J. Mater. Chem. C*, 2020, **8**, 8560–8566 | **8563**

Fig. 5 Characteristics of vacuum-processed OLEDs based on the naphthyridine TADF emitters (7 wt% in mCP): (a) EQE vs. luminance, (b) energy level diagram, (c) current density and luminance vs. applied voltage, and (d) normalized electroluminescence spectra.

Table 2 Main parameters of vacuum- and solution-processed OLEDs based on the ND(7 wt%):mCP emissive layer

Tech.	Emitter	V_{on}^{a} (V)	EQE^{b} (%)	L_{max} (cd m^{-2})	CE_{max} (cd A^{-1})	LE_{max} (lm W^{-1})	λ_{max} (nm)	FWHM (nm)	CIE 1931 (x, y)
Vac.	*t*Cz-ND	3.25	17.0/9.9/7.0	8424	22.17	19.88	459	66	(0.14, 0.16)
	Me*t*Cz-ND	3.25	17.6/14.4/12.5	21 459	31.98	23.60	481	88	(0.18, 0.32)
Sol.	*t*Cz-ND	4.30	13.5/12.1/7.8	6840	17.26	10.24	452	66	(0.15, 0.14)
	Me*t*Cz-ND	3.40	11.7/7.5/11.0	23 028	23.84	11.76	479	80	(0.16, 0.29)

[a] Turn-on voltage at 1 cd m^{-2}. [b] Maximum EQE/EQE at 100 cd m^{-2}/EQE at 1000 cd m^{-2}.

The main characteristics of the vacuum-processed OLEDs are provided in Fig. 5, meanwhile the key parameters are summarized in Table 2. Vacuum-processed devices were fabricated using the following layer configuration: ITO(100 nm)/ TAPC(30 nm)/TCTA(5 nm)/emitter(7 wt%): mCP(20 nm)/ DPEPO(5 nm)/TmPyPB(50 nm)/LiF(0.8 nm)/Al(100 nm), where the emitter was either *t*Cz-ND or Me*t*Cz-ND. An energy level diagram of the devices is displayed in Fig. 5b. 4,4′-Cyclo-hexylidenebis[*N*,*N*-bis(4-methylphenyl)benzenamine] (TAPC) and 4,4′,4″-tris(carbazol-9-yl)triphenylamine (TCTA) acted as hole injection and transport layers, respectively, whereas LiF and TmPyPB were employed for electron injection and transport, respectively. A thin 5 nm layer of DPEPO possessing a large HOMO–LUMO gap and a high triplet energy (3.0 eV) was used to confine excitons within the emissive layer.

OLEDs based on *t*Cz-ND demonstrated a low turn-on voltage (V_{on}) of 3.25 V, EL peak at 459 nm and FWHM of 66 nm rendering deep-blue narrow-band emission with Commission Internationale de L'Eclairage (CIE) coordinates of (0.14, 0.16). With these parameters, our device surpassed the recently

reported vacuum-processed OLED device based on the same naphthyridine compound.[16] Specifically, λ_{max} and FWHM of the current device were 10 nm smaller as compared to those of the previously reported device. This was mainly attributed to the proper device optimization carried out at 3 times lower emitter concentration (7 wt%) in the less polar mCP host (*versus* strongly polar DPEPO host). Moreover, as will be shown below, the *t*Cz-ND emitter was also confirmed to be suitable for fabrication of solution-processed deep-blue TADF OLEDs. The maximum EQE of *t*Cz-ND-based devices was 17% at low brightness and low current density (Fig. 5a). At the practically useful brightness of 100 cd m^{-2}, EQE decreased down to 9.9% with a further roll-off to 7% at 1000 cd m^{-2}. Maximum brightness achieved in this device was 8424 cd m^{-2}. A further increase of applied bias caused degradation of the device performance, most probably because of the exciton annihilation processes and loss of the current balance.

Although the Me*t*Cz-ND-based vacuum-processed OLEDs demonstrated similar turn-on characteristics with V_{on} = 3.25 V, EL of the devices was considerably redshifted with the EL peak at

8564 | J. Mater. Chem. C, 2020, 8, 8560–8566

This journal is © The Royal Society of Chemistry 2020

481 nm well matching the FL spectrum of the compound doped into mCP (Fig. 3). Additionally, the stronger CT character of **Me*t*Cz-ND** (as compared to that of ***t*Cz-ND**) also implied much broader EL emission of the device (FWHM = 86 nm) typical of conventional TADF emitters. The CIE coordinates of this device (0.18, 0.32) corresponded to sky-blue emission. Similar to ***t*Cz-ND** based OLEDs, the **Me*t*Cz-ND** based devices exhibited roughly the same maximum EQE of 17.6% at low brightness. However, in contrast to ***t*Cz-ND**, the latter demonstrated reduced efficiency roll-off. Explicitly, EQE was reduced only down to 14.4% and 12.5% at the brightness of 100 cd m^{-2} and 1000 cd m^{-2}, respectively. The device brightness maxed out at 21 459 cd m^{-2} still maintaining EQE above 4%.

The more rapid efficiency roll-off in the OLED based on ***t*Cz-ND** can be justified by the 3-fold longer τ_{DF} (8.8 μs) measured for this emitter as compared to that for **Me*t*Cz-ND**. Long triplet lifetimes are undesirable, since they increase the probability of triplet interaction causing detrimental annihilation effects. On the other hand, the fast rISC and short τ_{DF} (3.1 μs) of **Me*t*Cz-ND** significantly lowered the triplet population by rapid up-conversion to the singlet manifold resulting in only 29% loss of device efficiency at the brightness of 1000 cd m^{-2}. For comparison, the device based on ***t*Cz-ND** lost 60% of its initial efficiency at a similar brightness. It is worth noting that the maximum EQE values of ND-based OLEDs are in good agreement with the Φ_{FL} values obtained for the ND-doped mCP films, if ~20% light outcoupling efficiency of the devices (the case of random emitter orientation) is taken into account, *i.e.* EQE = 0.2 × Φ_{FL}.[22] This highlights the light outcoupling as the prime efficiency loss suggesting that the OLED structure is optimized at least for the low brightness regime. Compared to the performance of currently state-of-the-art narrow-band deep-blue (<460 nm) OLEDs based on conventional D–A-type TADF emitters, these ND-based (particularly ***t*Cz-ND**-based) OLEDs are among the best devices in terms of the EQE and efficiency roll-off properties (see Table S5 in the ESI†).[8,12,23–28] The results imply that sterically controlled CT interactions combined with H-bonding can indeed be promising in attaining narrow deep-blue TADF by employing ND acceptors.

Furthermore, both ND emitters were also tested in analogous solution-processed OLEDs in which TAPC and TCTA layers were replaced by solution-processable PEDOT:PSS and PVK (Fig. S5 in ESI† and Table 2). The performance of these OLEDs was found to be similar to that of the vacuum-processed devices at high current densities regardless of the inferior performance observed at low currents. The worsened performance in terms of the increased V_{on} and the reduced EQE can be attributed to the reduced homogeneity of the solution processed layers as compared to the vacuum evaporated ones and rather poor hole injection through PVK causing unbalanced electron and hole currents. Evidently, increasing the current density raises the EQE of the solution processed OLEDs almost up to the point of the vacuum-processed devices indicating that the injection regime close to optimal is achieved. Similar to the vacuum-evaporated OLEDs, the solution-processed devices based on ***t*Cz-ND** exhibited deep-blue (λ_{max} = 452 nm) and narrow-band

(FWHM = 66 nm) emission with an EQE of up to 13.5%, which could be of potential interest to display manufacturers.[29] Although **Me*t*Cz-ND** showed a higher Φ_{FL} (86%) as compared to that of ***t*Cz-ND** (76%), the solution-processed device based on **Me*t*Cz-ND** exhibited a slightly lower maximum EQE (11.7%) than that of the ***t*Cz-ND**-based device. This can be explained by the different EQE *vs.* luminance dependences observed for the two studied compounds (see Fig. S5a, ESI†), which suggest that the current imbalance is more pronounced for the **Me*t*Cz-ND**-based device causing a delayed rise in EQE and thus slightly reduced maximum EQE. Summing up, the demonstrated performance shows the suitability of the investigated naphthyridines to be employed also as solution-processable deep-blue TADF emitters.

4. Conclusion

In conclusion, relying on H-bonding and sterically controlled CT interactions, blue/deep-blue TADF emitters based on D–A-type carbazole–naphthyridine compounds have been developed. The ND compounds were found to express a small singlet–triplet energy gap (down to 0.09 eV), high fluorescence quantum yield (up to 0.86) and rather short delayed fluorescence lifetimes (down to 3.1 μs) resulting in a high rISC rate (up to 10^6 s^{-1}) when dispersed in the mCP host. The TADF properties and emission wavelength and band-width of the ND derivatives were mainly governed by the CT strength of the D–A interaction, which could be controlled *via* methyl substituents introduced at the first linking position of *t*-butyl-carbazole donors. The less sterically hindered compound ***t*Cz-ND** exhibited more narrow and shorter wavelength blue TADF as compared to that of the more twisted methyl-substituted compound **Me*t*Cz-ND,** implying a trade-off between the reduced rISC and improved emissive properties (λ_{max} and FWHM). Importantly, the ND compounds were demonstrated to be suitable as TADF emitters for realization of vacuum- and solution-processed TADF OLEDs with low efficiency roll-off in sky-blue (CIE$_{xy}$: 0.18, 0.32) and deep-blue (CIE$_{xy}$: 0.14, 0.16) spectral ranges. The optimized devices with 7 wt% ND emitter in the weakly polar mCP host delivered up to ~17.6% and ~13.5% EQEs for the vacuum- and solution-processed OLEDs, respectively. The OLEDs based on unsubstituted ***t*Cz-ND** exhibited deep-blue (λ_{max} < 460 nm) and narrow-band (FWHM = 66 nm) electroluminescence, whereas those based on more twisted methyl-substituted **Me*t*Cz-ND** expressed broader band (FWHM > 80 nm) and sky-blue (λ_{max} ≈ 480 nm) emission. The demonstrated ND-based TADF OLEDs are among the best blue/deep-blue-emitting devices in terms of EQE and efficiency roll-off properties. This highlights the potential of carbazole–naphthyridine-derived materials to become the basis in future engineering of deep-blue TADF emitters.

Conflicts of interest

The authors declare no conflict of interests.

This journal is © The Royal Society of Chemistry 2020

J. Mater. Chem. C, 2020, **8**, 8560–8566 | **8565**

Acknowledgements

References

1 Y. Im, M. Kim, Y. J. Cho, J. A. Seo, K. S. Yook and J. Y. Lee, *Chem. Mater.*, 2017, **29**, 1946–1963.

2 F. B. Dias, T. J. Penfold and A. P. Monkman, *Methods Appl. Fluoresc.*, 2017, **5**, 012001.

3 H. Uoyama, K. Goushi, K. Shizu, H. Nomura and C. Adachi, *Nature*, 2012, **492**, 234–238.

4 Z. Yang, Z. Mao, Z. Xie, Y. Zhang, S. Liu, J. Zhao, J. Xu, Z. Chi and M. P. Aldred, *Chem. Soc. Rev.*, 2017, **46**, 915–1016.

5 T. Serevičius, R. Skaisgiris, J. Dodonova, K. Kazlauskas, S. Juršėnas and S. Tumkevičius, *Phys. Chem. Chem. Phys.*, 2019, **22**, 265–272.

6 T. J. Penfold, F. B. Dias and A. P. Monkman, *Chem. Commun.*, 2018, **54**, 3926–3935.

7 Y. Liu, C. Li, Z. Ren, S. Yan and M. R. Bryce, *Nat. Rev. Mater.*, 2018, **3**, 18020.

8 L.-S. Cui, H. Nomura, Y. Geng, J. U. Kim, H. Nakanotani and C. Adachi, *Angew. Chem., Int. Ed.*, 2017, **56**, 1571–1575.

9 Y. J. Cho, S. K. Jeon, S. S. Lee, E. Yu and J. Y. Lee, *Chem. Mater.*, 2016, **28**, 5400–5405.

10 T. Hatakeyama, K. Shiren, K. Nakajima, S. Nomura, S. Nakatsuka, K. Kinoshita, J. Ni, Y. Ono and T. Ikuta, *Adv. Mater.*, 2016, **28**, 2777–2781.

11 P. Pander, A. Swist, R. Motyka, J. Soloducho, F. B. Dias and P. Data, *J. Mater. Chem. C*, 2018, **6**, 5434–5443.

12 P. Rajamalli, N. Senthilkumar, P.-Y. Huang, C.-C. Ren-Wu, H.-W. Lin and C.-H. Cheng, *J. Am. Chem. Soc.*, 2017, **139**, 10948–10951.

13 X. Zhou, H. Yang, Z. Chen, S. Gong, Z. H. Lu and C. Yang, *J. Mater. Chem. C*, 2019, **7**, 6607–6615.

14 Y. Lee, S. J. Woo, J. J. Kim and J. I. Hong, *Org. Electron.*, 2020, **78**, 105600.

15 C. Chen, H. Y. Lu, Y. F. Wang, M. Li, Y. F. Shen and C. F. Chen, *J. Mater. Chem. C*, 2019, **7**, 4673–4680.

16 Y.-F. Shen, W.-L. Zhao, H.-Y. Lu, Y.-F. Wang, D.-W. Zhang, M. Li and C.-F. Chen, *Dyes Pigm.*, 2020, **178**, 108324.

17 M. Budzynski, T. Baumann and D. Ambrosek, in *Organic Light Emitting Materials and Devices XXII*, ed. F. So, C. Adachi and J.-J. Kim, SPIE, 2018, vol. 10736, p. 51.

18 M. J. Adams, J. G. Highfield and G. F. Kirkbright, *Anal. Chem.*, 1977, **49**, 1850–1852.

19 E. Miyamoto, Y. Yamaguchi and M. Yokoyama, *Electrophotography*, 1989, **28**, 364–370.

20 M. J. Frisch, G. W. Trucks, H. B. Schlegel, G. E. Scuseria, M. A. Robb, J. R. Cheeseman, G. Scalmani, V. Barone, G. A. Petersson, H. Nakatsuji, X. Li, M. Caricato, A. Marenich, J. Bloino, B. G. Janesko, R. Gomperts, B. Mennucci, H. P. Hratchian, J. V. Ortiz, A. F. Izmaylov, J. L. Sonnenberg, D. Williams-Young, F. Ding, F. Lipparini, F. Egidi, J. Goings, B. Peng, A. Petrone, T. Henderson, D. Ranasinghe, V. G. Zakrzewski, J. Gao, N. Rega, G. Zheng, W. Liang, M. Hada, M. Ehara, K. Toyota, R. Fukuda, J. Hasegawa, M. Ishida, T. Nakajima, Y. Honda, O. Kitao, H. Nakai, T. Vreven, K. Throssell, J. J. A. Montgomery, J. E. Peralta, F. Ogliaro, M. Bearpark, J. J. Heyd, E. Brothers, K. N. Kudin, V. N. Staroverov, T. Keith, R. Kobayashi, J. Normand, K. Raghavachari, A. Rendell, J. C. Burant, S. S. Iyengar, J. Tomasi, M. Cossi, J. M. Millam, M. Klene, C. Adamo, R. Cammi, J. W. Ochterski, R. L. Martin, K. Morokuma, O. Farkas, J. B. Foresman and D. J. Fox, *Gaussian 09, Revision D.01*, Gaussian, Inc., Wallingford CT, 2013.

21 G. Kreiza, D. Banevičius, J. Jovaišaitė, K. Maleckaitė, D. Gudeika, D. Volyniuk, J. V. Gražulevičius, S. Juršėnas and K. Kazlauskas, *J. Mater. Chem. C*, 2019, **7**, 11522–11531.

22 N. C. Greenham, R. H. Friend and D. D. C. Bradley, *Adv. Mater.*, 1994, **6**, 491–494.

23 T. Serevičius, R. Skaisgiris, I. Fiodorova, V. Steckis, J. Dodonova, D. Banevičius, K. Kazlauskas, S. Juršėnas and S. Tumkevičius, *Org. Electron.*, 2020, 105723.

24 P. Rajamalli, D. Chen, W. Li, I. D. W. Samuel, D. B. Cordes, A. M. Z. Slawin and E. Zysman-Colman, *J. Mater. Chem. C*, 2019, **7**, 6664–6671.

25 Y. Im, S. H. Han and J. Y. Lee, *J. Mater. Chem. C*, 2018, **6**, 5012–5017.

26 M. Kim, S. K. Jeon, S.-H. Hwang and J. Y. Lee, *Adv. Mater.*, 2016, **28**, 603.

27 C. Chan, L. Cui, J. U. Kim, H. Nakanotani and C. Adachi, *Adv. Funct. Mater.*, 2018, **28**, 1706023.

28 D. H. Ahn, S. W. Kim, H. Lee, I. J. Ko, D. Karthik, J. Y. Lee and J. H. Kwon, *Nat. Photonics*, 2019, **13**, 540–546.

29 J. H. Lee, C. H. Chen, P. H. Lee, H. Y. Lin, M. K. Leung, T. L. Chiu and C. F. Lin, *J. Mater. Chem. C*, 2019, **7**, 5874–5888.